



FT-6876, a Potent and Selective Inhibitor of CBP/p300, is Active in Preclinical Models of Androgen Receptor-Positive Breast Cancer

Maureen Caligiuri¹ · Grace L. Williams¹ · Jennifer Castro¹ · Linda Battalagine¹ · Erik Wilker¹ · Lili Yao¹ · Shawn Schiller¹ · Angela Toms¹ · Ping Li¹ · Eneida Pardo¹ · Bradford Graves¹ · Joey Azoifeifa² · Agustin Chicas¹ · Torsten Herberitz¹ · Maria Lai² · Joel Basken² · Kenneth W. Wood¹ · Qunli Xu¹ · Sylvie M. Guichard¹

Accepted: 30 January 2023 / Published online: 24 February 2023
© The Author(s) 2023

Abstract

Background Patients with triple-negative breast cancer (TNBC) expressing the androgen receptor (AR) respond poorly to neoadjuvant chemotherapy, although AR antagonists have shown promising clinical activity, suggesting these tumors are AR-dependent. cAMP responsive element binding protein (CREB)-binding protein (CBP) and p300 are transcriptional co-activators for the AR, a key driver of AR+ breast and prostate cancer, and may provide a novel therapeutic target in AR+ TNBC.

Objectives The aim of this study was to determine the therapeutic potential of FT-6876, a new CBP/p300 bromodomain inhibitor, in breast cancer models with a range of AR levels in vitro and in vivo.

Methods Effects of FT-6876 on the CBP/p300 pathway were determined by combining chromatin immunoprecipitation (ChIP) with precision run-on sequencing (PRO-seq) complemented with H3K27 acetylation (Ac) and transcriptional profiling. The antiproliferative effect of FT-6876 was also measured in vitro and in vivo.

Results We describe the discovery of FT-6876, a potent and selective CBP/p300 bromodomain inhibitor. The combination of ChIP and PRO-seq confirmed the reduction in H3K27Ac at specific promoter sites concurrent with a decrease in CBP/p300 on the chromatin and a reduction in nascent RNA and enhancer RNA. This was associated with a time- and concentration-dependent reduction in H3K37Ac associated with a decrease in AR and estrogen receptor (ER) target gene expression. This led to a time-dependent growth inhibition in AR+ models, correlated with AR expression. Tumor growth inhibition was also observed in AR+ tumor models of TNBC and ER+ breast cancer subtypes with consistent pharmacokinetics and pharmacodynamics.

Conclusion Our findings demonstrate FT-6876 as a promising new CBP/p300 bromodomain inhibitor, with efficacy in preclinical models of AR+ breast cancer.

This work was presented in part at the Annual Meeting of the American Association for Cancer Research 2020 Virtual Meeting II; 22–24 June 2020.

Grace L. Williams, Jennifer Castro, Linda Battalagine, Lili Yao, Shawn Schiller, Angela Toms, Ping Li, Eneida Pardo, Bradford Graves, Agustin Chicas, Torsten Herberitz, Qunli Xu at the time this study was conducted.

✉ Sylvie M. Guichard
sguichard@formatherapeutics.com

¹ Forma Therapeutics, Inc, 300 N Beacon St, Watertown, MA 02472, USA

² Arpeggio Bio, Boulder, CO, USA

Key Points

FT-6876 reduced CBP/p300 activity and androgen receptor transcriptional activity, leading to antiproliferative activity in androgen receptor-positive breast cancer models in vitro and in vivo.

Mechanistically, FT-6876 blocks CBP/p300 binding to chromatin, affecting androgen receptor signaling and cell proliferation.

Dose-dependent pharmacokinetic/pharmacodynamic modulation resulting in tumor stasis in the androgen receptor-positive breast cancer model MDA-MB-453 was observed at well-tolerated doses of FT-6876, suggesting it is a promising therapeutic approach for androgen receptor-positive breast cancer.

1 Introduction

Breast cancer is a heterogeneous disease and has been classified into four major subtypes based on differential gene expression patterns, namely (1) luminal A (estrogen receptor-positive [ER+] and/or progesterone receptor-positive [PR+] human epidermal growth factor receptor 2 [HER2]-negative [HER2-]); (2) luminal B (ER+ and/or PR+ HER2+); (3) HER2-enriched (HER2 overexpression, ER- and PR-); and (4) basal-like/triple-negative breast cancer (TNBC; ER-, PR-, and HER2-) [1–3]. A subset of TNBC, the luminal androgen receptor (AR) type, is AR+ and expresses a gene signature reminiscent of ER+ luminal breast cancer [3, 4]. This has been shown to result from the binding of the AR to ER-specific cis-acting regulatory elements in a transcriptionally competent manner, leading to the expression of ER genes. This subset of breast cancers may be sensitive to the abrogation of AR transcriptional function [5].

TNBC accounts for approximately 10–20% of all breast cancers, and approximately 20–30% of those are AR+ [2, 6]. Preclinical and clinical data reports have provided an indication of the efficacy of anti-androgen therapies for AR+ TNBC [5, 7, 8]. In addition, biomarker-driven treatment strategies have led to the recent approvals of poly (ADP-ribose) polymerase (PARP) inhibitors and an immune checkpoint inhibitor for a subset of women with TNBC [9]. Despite these advances, luminal AR-subtype TNBC has a poorer prognosis compared with other types of TNBC and remains a high unmet medical need and an area of active therapeutic research [2, 10].

Studies have demonstrated that AR can substitute for ER and drive transcription of ER target genes, supporting TNBC tumor cell survival and proliferation [3, 11]. This AR-driven transcription is dependent on multiple essential co-factors, among which are the structurally related cAMP responsive element binding protein (CREB)-binding protein (CBP) and p300 [12, 13]. CBP and p300 are transcriptional co-activators for several oncogenic signaling pathways, including for AR and ER, that are implicated in the stimulation of tumor growth, apoptotic resistance, and angiogenesis [13–16]. Both CBP and p300 are large multidomain proteins, containing acetyl-lysine binding bromodomains (BRDs) and lysine acetyltransferase (HAT) domains [17, 18]. CBP and p300 are recruited to chromatin where they serve as a scaffold for the assembly of additional co-factors participating in the AR transcriptional complex [14, 16, 18, 19]. CBP/p300 catalyze the acetylation of histone and nonhistone proteins to regulate gene expression, protein stability, and other cellular functions. The BRD is essential to the histone acetyltransferase activity of CBP/p300 that augments coactivation for AR signaling [20, 21]. In addition, the CBP/p300 complex

has been shown to interact directly with AR at both the N- and C-terminus (including truncated forms of AR that lack the ligand-binding domain) [22–24] and to acetylate AR on lysine residues (K630, K632, and K633) in the hinge region, thereby stabilizing the receptor [14, 25, 26].

Since ARs must complex with co-activator proteins to drive target gene expression, inhibitors of these transcriptional co-activators provide potential alternative therapeutic targets beyond antagonists of ligand binding [20]. This may be particularly pertinent for AR+ tumors that are resistant to androgen antagonists due to the expression of splice variants, such as the AR-v7, which lack the ligand-binding domain [27, 28]. The CBP/p300 complex has emerged as a promising therapeutic target, along with several inhibitors in development that target either the HAT region or the BRD [20, 28–31].

In this study, we describe the discovery of FT-6876, a novel, small-molecule inhibitor of the BRD of CBP/p300, and present preclinical data demonstrating the antitumor activity of FT-6876 in AR+ breast cancer cell lines and patient-derived xenograft (PDX) models.

2 Methods

2.1 Study Design

The overall objectives of this study were to discover novel compounds that can inhibit acetylated lysine-containing proteins from binding to the BRDs of CBP/p300 proteins, and subsequently to assess the potential to inhibit AR+ breast cancer. Except where indicated, all experiments were conducted at Forma Therapeutics, Inc. (Watertown, MA, USA).

2.2 Chemicals

Experimental synthesis procedures for FT-6876 are described in detail in the following patent filings: WO2019055869, WO2019055877, WO2020006483, US20200002332, and WO2020190791. The synthetic AR agonist R1881 (metribolone) was obtained from Sigma-Aldrich (St Louis, MO, USA), and enzalutamide was purchased from MedChemExpress (Monmouth Junction, NJ, USA). All compounds were dissolved in dimethylsulfoxide (DMSO) and used at the concentrations indicated.

2.3 Bromodomain Assays

The potency of CBP/p300 inhibitors was determined using time-resolved fluorescence resonance energy transfer (TR-FRET) biochemical assays with CBP and p300.

BRD-containing proteins bind acetylated lysines on histone and nonhistone proteins. In the TR-FRET assays,

test compounds compete with the ligand for BRD binding, thereby reducing the TR-FRET signal. The assay was built using a glutathione-S-transferase (GST) fusion protein with the BRDs of CBP, p300, and BRD4, and a fluorescein amidites-labeled acetylated histone peptide. The addition of a terbium-labeled anti-GST antibody creates a FRET signal when the labeled histone peptide is bound to the BRD. The presence of a compound interacting with the BRD of the target protein displaces the labeled histone peptide, interrupting the FRET signal.

Nanoliter quantities of CBP/p300 inhibitors in 10-point, threefold serial dilutions in DMSO were predispensed into 1536-well assay plates. All assays were performed in a final volume of 6 μ L in assay buffer containing 50 mM HEPES, 0.5 mM glutathione, 0.01% bovine gamma globulin, 0.005% bovine serum albumin (BSA), and 0.01% Triton X-100. The highest concentration of compound and final concentrations of protein and ligands for the three assays are shown in Table 1. Assay plates were pre-stamped with compound, and 3 μ L of protein ($\times 2$) and 3 μ L of peptide ligand ($\times 2$) were added. Prior to measuring the FRET signal, plates were incubated at room temperature for the times shown in Table 1. The TR-FRET signal was read on the PHERAstar microplate reader with a homogeneous time-resolved fluorescence optic module (337/520/490) [BMG LABTECH Inc., Cary, NC, USA].

For all assays, data were reported as percentage inhibition compared with control wells. The half maximal inhibitory concentration (IC_{50}) values were determined by curve fitting of the standard four-parameter logistic fitting algorithm included in the Activity Base software package: IDBS XE Designer Model 205, and data were fit using the Levenburg Marquardt algorithm.

AlphaScreenTM was used to determine the IC_{50} against a range of 10 BRD-containing proteins representing the various branches of the BRD tree. AlphaScreen assays were conducted at Reaction Biology (Malvern, PA, USA) following

the procedure described previously [12]. The buffer for BRD was 50 mM HEPES-HCl, pH 7.5, 100 mM NaCl, 0.1% BSA, 0.05% 3-[(3-cholamidopropyl) dimethylammonio]-1-propanesulfonate, and 1% DMSO. Ligands were histone H4 peptide (1–21) K5/8/12/16Ac-Biotin, histone H3 (1–21) K9/14Ac-Biotin-OH, and histone H3 (1-30) K14/18/23/27Ac-GG-Biotin. FT-6876 was tested in 10-dose IC_{50} mode with threefold serial dilutions starting at 10 μ M against ATAD2, BPTF (PHD-BRD), BRD4-T, BRPF3, BRWD1-2, CECR2, CREBBP, SMARCA4, SP140, and TAF1-2. Control compounds (JQ-1, bromosporine, SGC-CBP30, PFI-3) were tested in 10-dose IC_{50} with threefold serial dilution starting at 10, 25, 50, 75, or 100 μ M. The IC_{50} curve was fit using GraphPad Prism 4 software (GraphPad Prism, La Jolla, CA, USA).

2.4 Western Blot, High-Content Analysis

The effect of FT-6876 on H3K27Ac in MDA-MB-453 cells was evaluated by Western blot and a high-content assay. For the Western blots, cells were exposed to a range of concentrations of FT-6876 for the indicated periods: 24 h for the dose response or 1, 2, 4 or 8, or 24 h for the time course. MDA-MB-453 cells were plated at 300,000 cells per well in a six-well dish in Leibovitz's L-15 medium supplemented with 10% fetal bovine serum (FBS; Gibco, USA). For the wash-off arm of the study, cells were treated with FT-6876 for 24 h and then incubated in the absence of compound for an additional 24 or 48 h prior to the preparation of lysates. For the washout study, MDA-MB-453 cells were exposed to DMSO or FT-6876 for 24 h and then washed off for 24 and 48 h prior to preparation of lysates. Lysates were prepared in E-PAGE loading buffer (Invitrogen, Waltham, MA, USA), boiled for 10–15 min, and analyzed by Western blot. The antibodies (Cell Signaling) were diluted 1:1000 for anti-H3K27Ac (clone D5E4), 1:2000 for anti-total H3 (clone 3H1), and 1:10,000 for anti- β -actin (clone AC-74).

Table 1 Concentration of assay components and incubation times

Assay target	CBP	p300	BRD4
FT-6876 highest concentration	1.7–4.2 μ M	1.7 μ M	33 μ M and subsequent half-log dilutions
Final protein concentration	0.5 nM CBP (N-terminal GST-CREBBP [aa1081-1197])	2.5 nM p300 (N-terminal GST-p300 [aa1040-1161])	1.5 nM BRD4 tandem domains
Final concentrations of ligands	25 nM tetra-acetylated H3 peptide* and 0.5 nM anti-GST-terbium	12.5 nM tetra-acetylated H3 peptide* and 0.5 nM anti-GST-terbium	10 nM tetra-acetylated H4 peptide [†] and 0.5 nM anti-GST-terbium
Incubation time (RT)	2 h	2 h	2–4 h

aa amino acid, RT room temperature

*ARTKQTARKSTGG(KAc)APR(KAc)QLAT(KAc)AAR(KAc)SAPGG(K5Fam)

[†]SGRG(KAc)GG(KAc)GLG(KAc)GGA(KAc)RHRKVGG(K5Fam)

The secondary antibodies were anti-rabbit IgG, DyLight 800 diluted 1:10,000 (SeraCare Life Sciences, Milford, MA). The blots were scanned and analyzed on a LI-COR Odyssey image analyzer. H3K27Ac levels were normalized to β -actin.

For the high-content assay, MDA-MB-453 cells were plated in a 96-well plate with black walls and a clear bottom and treated with 0.3 mM FT-6876 or DMSO for 24 h. Paraformaldehyde (Electron Microscopy Sciences, Hatfield, PA, USA) was added to a final concentration of 4%, and the cells were incubated for 15 min at room temperature. The cells were washed with phosphate-buffered saline (PBS) ($\times 3$) and then blocked/permeabilized with 0.5% Triton and 1% BSA in PBS for 1 h at room temperature. The cells were washed in PBS ($\times 3$) prior to adding anti-H3K27Ac Alexa 647 antibody (Cell Signaling) with 4',6-diamidino-2-phenylindole Alexa 385 (ThermoFisher, Waltham, MA, USA) and Texas Red-X phalloidin Alexa 591/608 in PBS/0.1%, Triton 1%, BSA, and incubating overnight at 4 °C. The cells were washed with PBS ($\times 3$) and read on a CellInsight CX7 High-Content Imager (ThermoFisher Scientific, Waltham, MA, USA).

2.5 Gene Expression Assays

For quantitative polymerase chain reaction (qPCR) assays, MDA-MB-453 cells were adapted to growth at 37 °C, 5% CO₂ in minimal essential media with 10% FBS, 2% L-glutamine, 1% non-essential amino acids, 1 mM sodium pyruvate, and 1.5 g/uL sodium bicarbonate. Cells were plated at 0.5 million cells/well in a six-well dish and incubated for 24 h to allow attachment. On day 1, the medium was replaced with a formulation containing 10% charcoal-stripped serum, and the cells were incubated for an additional 5 days. The cells were then treated with 10 nM R1881 for 24 h, washed with PBS ($\times 1$), and treated with either 0.156, 0.625, or 2.5 μ M FT-6876, or 0.1% DMSO for an additional 24 h. RNA was prepared using the RNeasy Mini RNA isolation kit with a Qiacube according to the manufacturer (Qiagen, Hilden, Germany). A two-step RT-qPCR was performed using cDNA prepared using the iScript cDNA synthesis kit (Bio-Rad, Hercules, CA, USA) and TaqMan Fast Advanced Master Mix (ThermoFisher) and TaqMan gene expression assays (Invitrogen, Waltham, MA, USA). A total of 100 ng complementary DNA (cDNA) was used per qPCR reaction, and the delta-delta-Ct comparative method was used to analyze the modulation of gene expression in the treated groups versus DMSO.

RNA sequencing (RNA-Seq) was carried out on RNA prepared from MDA-MB-453 cells treated with 2 μ M FT-6876 for 24 h. Sequencing libraries were prepared with TruSeq Stranded mRNA Library Preparation kits and were subjected to Illumina sequencing (Q² Solutions EA Genomics). PRO-Seq was performed as previously described [32].

Chromatin immunoprecipitation and sequencing (ChIP-Seq) was performed on MDA-MB-453 cells treated with FT-6876 (Active Motif, Carlsbad, CA, USA). MDA-MB-453 cells were cultured in charcoal-stripped serum for 5 days, challenged with 10 nM R1881 for 24 h, and then exposed to 2 μ M FT-6876 for 24 h. The cells were fixed in 1.1% formaldehyde solution with 10 mM NaCl, 5 mM HEPES, and 0.1 mM EDTA for 15 min at room temperature. Fixation was stopped with 0.125 M glycine, and the cells were snap frozen in 0.5% Igepal/PBS with 1 mM phenylmethylsulfonyl fluoride. Immunoprecipitation was carried out on 30 mg chromatin with anti-H3K27Ac (Active Motif; catalog # 39133), anti-CBP (Cell Signaling Technology, Danvers, MA, USA; catalog # 7425BF), or anti-p300 (Santa Cruz Biotechnology, Dallas, TX, USA; catalog # sc-585). Sequencing was performed using the Illumina NextSeq 500 System.

2.6 Proliferation and Washout Assays

MDA-MB-453 cells were purchased from the American Type Culture Collection (ATCC, Manassas, VA, USA) and cultured in L-15 media supplemented with 10% FBS in atmospheric air. For the colony formation assay, 3000 cells/well were plated in a 12-well dish and incubated overnight for adherence. The following day, FT-6876 (nine-point titration, final highest concentration 10 μ M, half-log dilution) was added to the cells, which were subsequently incubated for 5 or 10 days continuously. For the washout arm of this study, cells were exposed to compound for the indicated period of 1, 3, or 5 days before the cells were washed with PBS and compound-free media were added to each well. Incubation of the cells was continued for a total of 10 days. The impact of FT-6876 on colony formation was determined by staining with a crystal violet solution. Results are averages of two independent experiments. In both arms of the study, the growth inhibitory effect was assessed by the concentration inhibiting growth by 50% (IC₅₀) using a nonlinear regression equation and a variable slope (GraphPad Prism).

A CellTiter-Glo[®] 2.0 (CTG) assay (Promega, Madison, WI, USA) was used to determine the effects of FT-6876 and enzalutamide on the viability of MDA-MB-453 cells after 10 days of treatment. MDA-MB-453 cells were plated at 3000 cells/well in a 96-well cell culture plate and incubated overnight for adherence. FT-6876 and enzalutamide were tested in a threefold, nine-point titration with a top dose of 10 μ M for FT-6876 and 30 μ M for enzalutamide in triplicate. Cells were incubated for 10 days, with media and test compounds replenished on day 5. Plates were read on the EnSpire plate reader (PerkinElmer, Waltham, MA, USA). IC₅₀ values were determined, and dose-response curves were generated using nonlinear regression analyses in XLFit.

Proliferation assays were conducted in a panel of breast cancer cell lines with a range of AR mRNA expression, at

Pharmaron, Inc. (Beijing, China). Breast cell lines were obtained from the ATCC and DSMZ (German Collection of Microorganisms and Cell Cultures GmbH) and cultured according to the distributor's recommendations. Cells were plated at a density of 300–3000 cells/well, depending on the proliferation rate of the cell line, in 96-well plates in triplicate and allowed to attach overnight. The following day, cells were exposed to FT-6876 continuously for 10 days. Media were replaced every 3 days with fresh compound. At the end of the incubation period, cell viability was assessed using the CTG assay. The growth inhibitory effect was assessed using the concentration that inhibited growth by 50%, a nonlinear regression equation, and a variable slope (XLFit); each value represents the average result from two independent experiments. The mRNA expression for the AR (HUGO: AR) was downloaded from <https://depmap.org/portal/gene/AR?tab=characterization> (release 21Q4) and aligned to the IC₅₀ values obtained for the cell lines tested (note no AR expression for MFM-223; electronic supplementary material [ESM] Table S1).

2.7 In Vivo Studies, Animal Models

For all studies using experimental animals, the animals' care was in accordance with institutional guidelines.

2.8 Pharmacology

The pharmacodynamic effects of a single dose of FT-6876 in MDA-MB-453 xenografts were evaluated at Pharmaron (Beijing, China). All the procedures related to animal care were performed according to guidelines approved by the Institutional Animal Care and Use Committee of Pharmaron following the guidance of the Association for Assessment and Accreditation of Laboratory Animal Care.

The MDA-MB-453 tumor cell line was maintained in vitro as a monolayer culture in a modified L-15 medium supplemented with 10% heat-inactivated FBS at 37 °C in atmospheric air. The tumor cells were routinely subcultured once a week using trypsin-EDTA treatment so as not to exceed four to five passages. The cells growing in an exponential growth phase were harvested and counted for tumor inoculation.

Female nonobese, diabetic, severe combined immunodeficiency (NOD SCID) mice aged 6–8 weeks (body weight 18–22 g) were obtained from Beijing AniKeeper Biotech Co., Ltd (Beijing, China). For tumor development, each mouse was inoculated subcutaneously on the right flank with MDA-MB-453 cells (1×10^7) in 0.1 mL of 1:1 L-15 Medium/Matrigel mixture (BD Biosciences). Treatments were started when the mean tumor volume reached ~319 mm³. Mice were administered 10, 30, or 100 mg/kg FT-6876, or vehicle, as a single oral dose made up to a

volume of 10 mL/kg. Vehicle was 0.5% carboxymethylcellulose (CMC), 0.5% Tween 80 (Sigma-Aldrich) pH 8.0. All study animals were monitored for body weight.

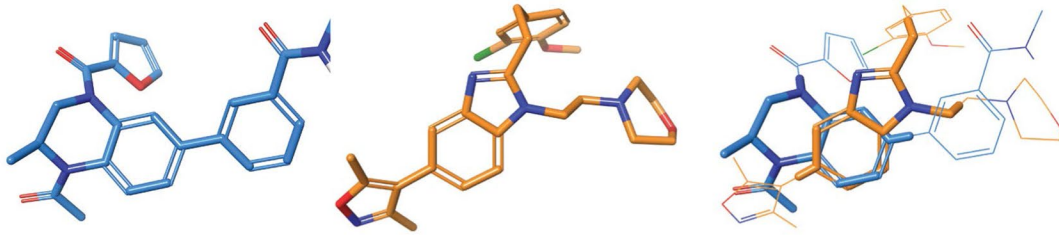
Plasma and tumor samples were collected at different time points throughout 24 h after oral administration. Plasma samples and tumor samples were used for pharmacokinetic and pharmacodynamic measurements, respectively. The liquid chromatography-tandem mass spectrometry method was used to determine the drug concentration in plasma. H3K27Ac was measured by Western blot, and ER/AR target genes (*XBPI*, *SPDEF*) were assessed by qPCR. All gene expression was normalized to *GAPDH* expression.

For analysis of tumor volume, treatments were started when the mean tumor volume reached ~160 mm³. Tumor-bearing mice were staged by tumor size and assigned to treatment groups so that each group had an equivalent distribution of tumor sizes. FT-6876 was administered once per day on a 4 days on/3 days off schedule for 39 days. Tolerability was assessed by daily body weight measurements and any abnormal effects or clinical signs. Tumor size was measured twice weekly with a caliper. The group mean and standard deviation were calculated for tumor volume and body weight.

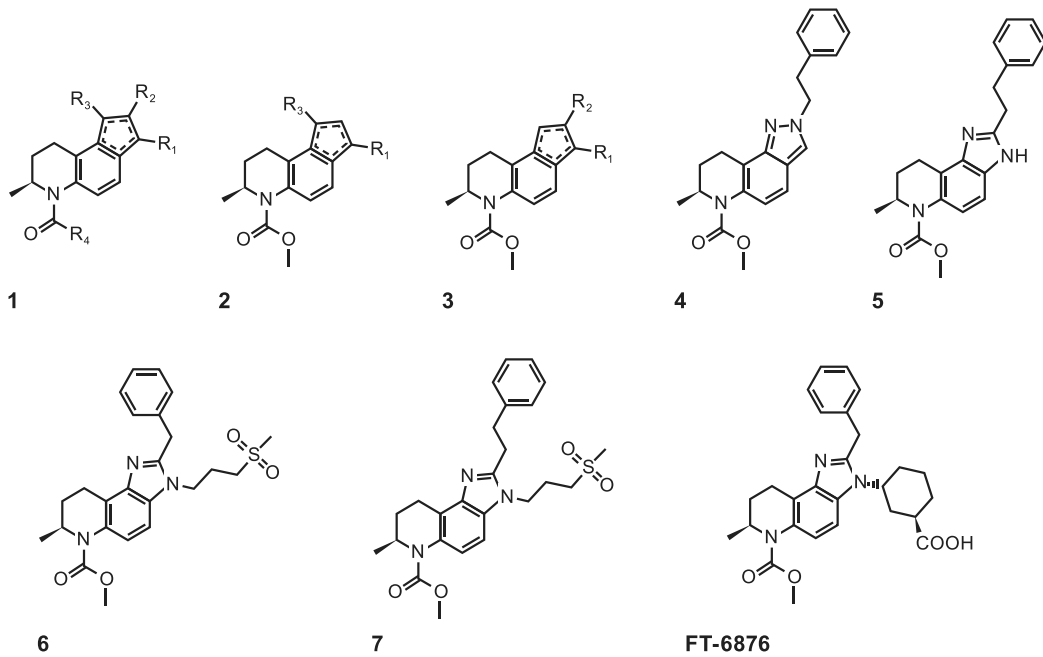
2.9 PDX Screen

An efficacy screen of FT-6876 in a panel of human breast cancer PDX (XenoSTART-PDX, San Antonio, TX, USA) models in immune-deficient mice was conducted at South Texas Accelerated Research Therapeutics, LLC (San Antonio, TX, USA). The PDX tumors were established by passage of tumor fragments (~70 mg) subcutaneously into 6- to 12-week-old female CB-17 SCID and athymic nude mice, obtained from Charles River Laboratories (Wilmington, MA, USA). Tumors were monitored until they reached a mean tumor volume of 125–150 mm³; animals were then randomized (stratified by tumor volume) to vehicle (0.5% CMC, 0.5% Tween80, pH 8.5; pH 8.0) prior to dosing or a 50 mg/kg oral dose of FT-6876 4 days per week for 45 days. Each model included eight animals treated with vehicle and one animal treated with FT-6876. For hormone-dependent models, animals were supplemented with exogenous estradiol via drinking water throughout the duration of the study. All animals received fresh DietGel[®] supplementation, daily, throughout the duration of the study. Tumor size and body weight were measured twice per week. Tumor growth inhibition (TGI) was calculated as follows: $(\%TGI = 1 - (TV[FT - 6876]_{final} - TV[FT - 6876]_{initial}) / (TV[vehicle]_{final} - TV[vehicle]_{initial}))$ where TV is tumor volume. ER and AR expression were evaluated using immunohistochemistry on PDX TMA (Invitrogen Cat# MA5-14501 and Novus Cat# NBP2-12502, respectively).

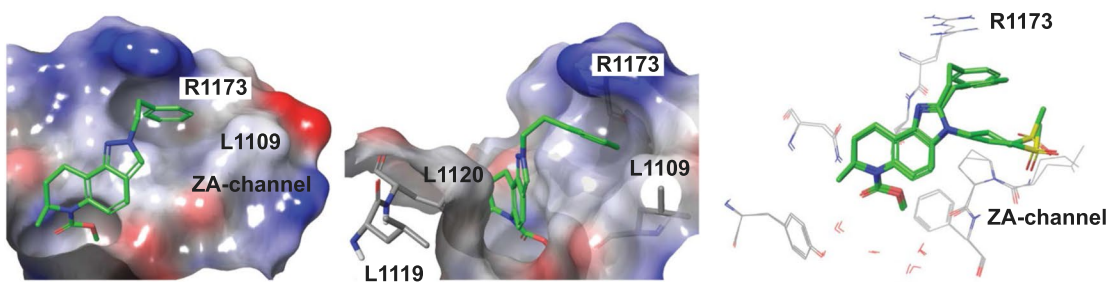
a



b



c



d

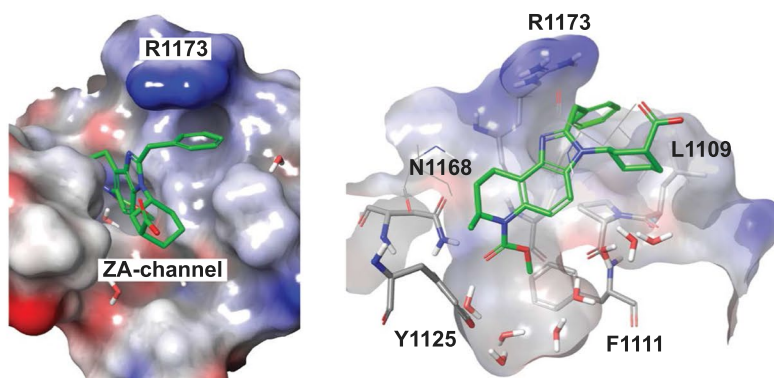


Fig. 1 FT-6876 is a pentacyclic carboxylic acid inhibitor of the bromodomains of CBP and p300. **a** Aligned crystal structures 5VOM (left: with a BZP BRD4 ligand in blue) and 4NR7 (middle: with SGC-CBP30 in orange). The right: common phenyl ring in both cores with adjacent overlapping functionality. **b** Structures leading to development of FT-6876. **c** The crystal structure of 4 suggested that projecting moieties into the ZA channel to fill the lipophilic space between L1109 on one side, and L1119 and L1120 on the other side, could provide productive hydrophobic binding contacts affecting potency and selectivity. **d** X-ray crystal structure of FT-6876 in complex with the BRD of CBP. Left: the central imidazo tetrahydroquinoline core of FT-6876 binds a narrow cleft and projects the 2-benzyl substituent onto a lipophilic surface beneath the guanidine moiety of R1173. The cyclohexane carboxylic acid reaches into the wider ZA channel; right: key recognition features of FT-6876 include the conserved N1168 (bi-dentate hydrogen bond with carbamate) and a key structural water molecule that also binds Y1125. *BZP* benzylpiperazine, *BRD* binding bromodomain

Reference samples were used to determine the threshold H score for positivity. HER2 status was from XenoSTART.

2.10 Statistical Analyses

Except where indicated, results are presented as mean and standard deviation and were calculated using GraphPad Prism. For all statistical analyses, $p < 0.05$ was considered significant.

3 Results

3.1 Discovery of FT-6876

FT-6876 was discovered using a de novo design approach. The previously described compound Structural Genomics Consortium (SGC)-CBP30 is a selective CBP/p300 binder with 40-fold selectivity over BRD4 and other BRD and bromodomain extraterminal domain (BET) family members but has poor microsomal stability [33–35]. Even weak binders (1–10 μM) to BET bromodomains elicit robust biological effects in cells and in vivo (crystal structures of DMSO or *N*-methyl-2-pyrrolidone [NMP] bound to BRD4 or CBP [Protein Data Bank identification: 3P1D, 4IOR, 4J1P], and resveratrol or RVX-208 are only μM binders) [24, 34, 36–41]. To clearly define the biologic/pharmacologic effect of binding to the BRD of CBP/p300 and understand its effect on HAT activity, we designed CBP/p300 BRD binders with very high selectivity over BET and other BRDs.

Overlays of proprietary crystal structures for benzylpiperazine (BZP) and tetrahydroquinoline (THQ)-derived BET ligand scaffolds with SGC-CBP30 showed high congruity with the central phenyl ring common to both ligand classes (Fig. 1a).

Modeling studies established that a five-membered heteroaryl ring fused to this core phenyl group, exemplified

by structure 1 in Fig. 1b, could provide suitable vectors by which to append CBP/p300-BRD compatible moieties and explore R1 (ZA channel) and either R2 or R3 (lipophilic area underneath R1173). Examples with distinct connectivity, such as 2 (R1/R3) and 3 (R1/R2) in Fig. 1b, were synthesized and yielded a spectrum of CBP affinities and selectivity over BRD4. A crystal structure of compound 4 in Fig. 1b (CBP $\text{IC}_{50} \sim 2 \mu\text{M}$; BRD4 $> 25 \mu\text{M}$) validated the general design hypothesis (Fig. 1c). The crystal structure of 4 (Fig. 1b) suggested that projecting moieties into the ZA channel to fill the lipophilic space between L1109 on one side and L1119 and L1120 on the other side could provide productive hydrophobic binding contacts that affect potency and selectivity.

Moving from an indazole to an imidazole provided options to tether substitution to explore the ZA channel in a synthetically more facile way. Examples such as 6 or 7 (Fig. 1b) bound CBP in a consistent manner with an attached propyl methyl sulfone occupying a similar area and a methylene or ethano-linked phenyl group slotting in comparable fashion underneath R1173. Moieties such as the alkyl methyl sulfones, and other heteroatom-containing groups, including polar and basic functions, yielded varying degrees of selectivity and microsomal stability. It was the unprecedented inclusion of acidic groups as part of projecting a five- to six-membered ring in the ZA channel that delivered substantial increases in both selectivity over BET BRD binding and enhanced rodent and human microsomal stability. Among the various changes evaluated, the addition of a 3(R)-carboxy moiety to a cyclohexyl ring generated FT-6876; it maintained potency while solubility and microsomal stability improved due to a reduction in lipophilicity ($\log D = 2.2$). X-ray crystal structure of FT-6876 complexed with the BRD of CBP confirmed that the central imidazo THQ core of FT-6876 binds a narrow cleft and projects the 2-benzyl substituent onto a lipophilic surface beneath the guanidine moiety of R1173 (Fig. 1d). The cyclohexane carboxylic acid reaches into the wider ZA channel. Key recognition features of FT-6876 include the conserved residue N1168 (bi-dentate hydrogen bond with carbamate) and a key structural water molecule that also binds Y1125.

3.2 FT-6876 is a Potent, Selective, CBP/p300 Bromodomain Inhibitor

The potency and selectivity of CBP/p300 inhibition was determined using TR-FRET biochemical assays. Results showed that FT-6876 is a potent inhibitor of tetra-acetylated histone H3 binding to the BRDs of CBP and p300, with IC_{50} values of 0.005 and 0.002 μM , respectively. Good selectivity was observed over other BRD-containing proteins, with > 400 -fold selectivity against BRD4 (IC_{50} value 2.32

μM) (Table 2). FT-6876 was found to be highly selective against other BRDs representing branches of the BRD tree, including >5000-fold selectivity against BRD9 (IC_{50} value 26.7 μM).

3.3 FT-6876 Reduces H3K27 Acetylation in MDA-MB-453 Cells

CBP and p300 are histone acetyltransferases that modify histone and nonhistone proteins at specific lysine residues. Histone H3 is a core component of the nucleosome and is acetylated at lysine 27 (H3K27Ac) by CBP/p300. Inhibition of CBP/p300 leads to a reduction in H3K27Ac, which can in turn inhibit transcription as the chromatin converts from an open, transcriptionally active form to a compact form that is less transcriptionally active.

MDA-MB-453 cells were exposed to a range of FT-6876 concentrations for 24 h, and the impact on H3K27Ac was assessed by Western blot. A concentration-dependent reduction in this histone marker was observed, with substantial reduction evident at 0.10 μM , the lowest concentration tested (Fig. 2a). These results were confirmed using high-content image analysis, which showed a reduction in H3K27Ac across the population of the cells. A uniform reduction (53% of control) in H3K27Ac occurred following treatment with 0.3 μM FT-6876 (Fig. 2b). FT-6876 induced the rapid reduction in H3K27Ac, as demonstrated by Western blot, after 1 h of exposure (Fig. 2c). We tested the persistence of the

reduction in H3K27Ac in a compound washout study, in which cells were exposed to FT-6876 for 24 h followed by wash-off. Levels of acetylation returned to baseline by 24 h post removal of the compound, indicating the reduction in acetylation was reversible and reflecting the dynamic state of histone acetylation in the cell (Fig. 2d).

3.4 FT-6876 Modulates Estrogen Receptor (ER) and Androgen Receptor (AR) Gene Expression in MDA-MB-453 Cells

Our hypothesis was that modulation of CBP/p300 with FT-6876 alters chromatin compaction and, when in the vicinity of AR-responsive genes, selectively reduces AR transcriptional activity at these loci. The TNBC cell line MDA-MB-453 expresses high levels of AR, making it particularly useful for studying androgen regulation of gene expression. If the proposed mechanism of action of FT-6876 on AR and ER signaling is correct, the impact on the expression of genes related to AR and ER signaling should be preferentially affected compared with other genes expressed in MDA-MB-453 cells. RNA-Seq was performed on MDA-MB-453 cells treated with FT-6876 for 24 h. Gene set enrichment analysis (GSEA; 50 hallmarks of cancer pathways) of the RNA-Seq data is shown in Fig. 3a. This confirmed the activity of FT-6876 in targeting AR and ER signaling with a significant modulation of the pathway over 24 h, in addition to cell cycle-related genes including the E2F and Myc pathways (corrected p -values = 10^{-8} to 10^{-10}).

In AR-expressing TNBC cells, the transcriptional signature of ER has been shown to be orchestrated by the AR and dependent on FoxA1 [3]. The effect of FT-6876 on AR and ER transcription was validated by examining the effect of the compound on AR and ER target genes using qPCR. When MDA-MB-453 cells were exposed to the synthetic AR agonist R1881 (metribolone), the impact on the AR target gene *SPDEF* and ER target gene *AQP3* was evaluated. Both *SPDEF* and *AQP3* were upregulated by R1881, and the induced expression of these genes was reduced by treatment with FT-6876 (Fig. 3b). Taken together, the data demonstrate that FT-6876 modulates AR and ER target genes in a concentration-dependent manner in the TNBC model MDA-MB-453.

To further evaluate the mechanism of action of FT-6876, it was desirable to determine whether the compound would displace CBP and/or p300 at sites where a reduction in H3K27Ac and subsequent reduction in gene expression were observed. MDA-MB-453 cells were exposed to FT-6876 and analyzed using ChIP-Seq with anti-acetylated H3K27, CBP, and p300 antibodies. One of the genes of interest was the ER target gene *AQP3* that, as shown above, was upregulated following R1881 exposure and downregulated in the presence of FT-6876. In the promoter region of *AQP3*, R1881

Table 2 Potency and selectivity against other bromodomains

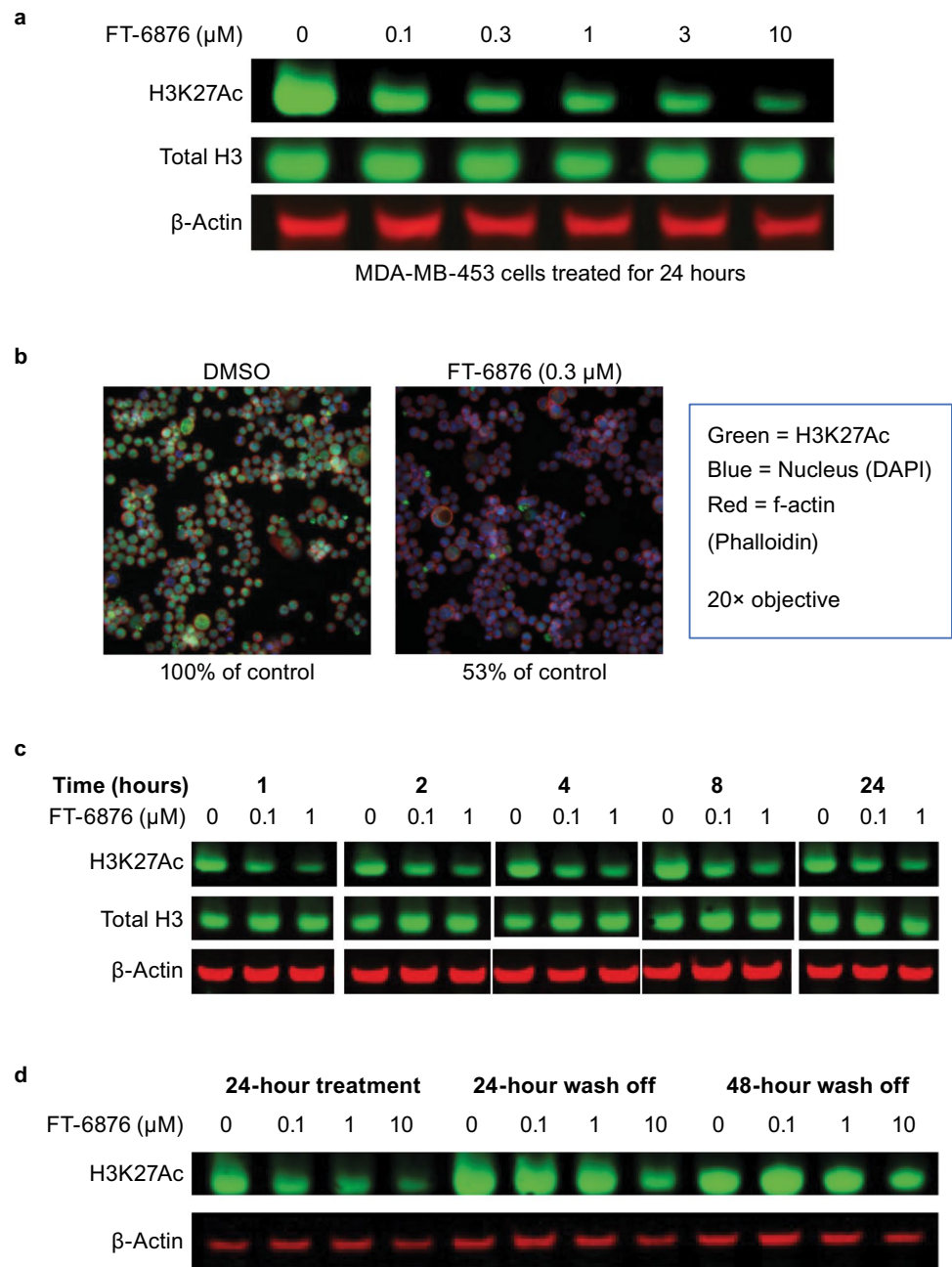
Bromodomain (TR-FRET assay)	FT-6876 IC_{50} (μM)
CBP	0.005
p300	0.002
BRD4	2.32
Bromodomain	FT-6876 IC_{50} (μM)
CBP ^a	0.06
BRD4 ^a	5.7
TAF1-2 ^a	8.7
ATAD2 ^a	> 10
BPTF ^a	> 10
BRPF3 ^a	> 10
BRWD1 ^a	> 10
CECR2 ^a	> 10
SMARCA4 ^a	> 10
SP140 ^a	> 10
BRD9 ^b	26.7
ASH1L ^b	> 30
BRWD3 ^b	> 30

IC_{50} half maximal inhibitory concentration, TR-FRET time-resolved fluorescence resonance energy transfer

^aAlphaScreenTM

^bTR-FRET assay

Fig. 2 FT-6876 reduces H3K27Ac in MDA-MB-453 cells. **a** Reduction in H3K27Ac after exposure to increasing concentrations of FT-6876. Representative Western blot of MDA-MB-453 cells exposed to DMSO or FT-6876 at the indicated concentrations for 24 h. **b** Uniform reduction on H3K27Ac in cells after exposure to FT-6876. Representative high-content image shows MDA-MB-453 cells treated with DMSO or 0.3 μ M FT-6876 for 24 h. **c** Rapid reduction in H3K27Ac after exposure to FT-6876. Western blot target engagement time course of MDA-MB-453 cells exposed to DMSO or FT-6876 at the indicated concentrations for 1, 2, 4, 8, or 24 h. **d** H3K27Ac reduction returned to baseline following removal of the compound. *DAPI* 4',6-diamidino-2-phenylindole, *DMSO* dimethylsulfoxide

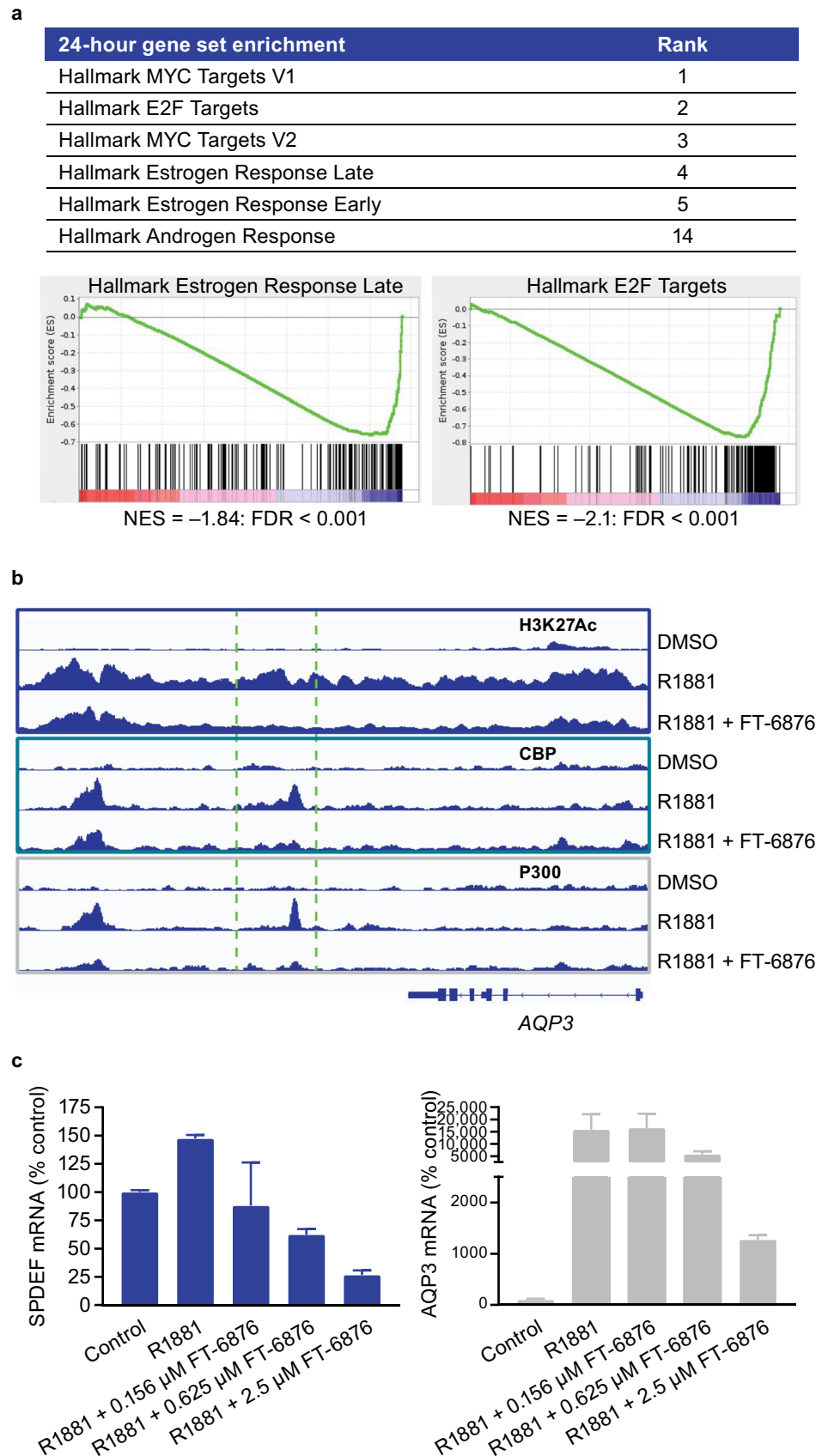


increased H3K27Ac at CBP and p300 overlapping peaks (Fig. 3c), coincident with the increased expression of *AQP3*. The addition of FT-6876 reduced H3K27Ac, concurrent with a reduction in CBP and p300 binding as well as a reduction in *AQP3* expression. The results support the hypothesis that displacement of CBP and p300 from the chromatin reduces local H3K27Ac and leads to decreased target gene expression. Notably, this region was confirmed as a binding site for ER based on the CistromeDb public database (available online at <http://cistrome.org/db/#/>).

Inhibition of CBP/p300 markedly impacts gene transcription by RNA polymerase II [42]. To assess the immediate

effects of CBP/p300 inhibition on gene transcription in MDA-MB-453 cells, we performed precision run-on followed by sequencing (PRO-Seq) in cells treated with either a DMSO control or FT-6876 at 2 μ M. Cells were harvested 1 h after exposure to DMSO or FT-6876 to assess the immediate and primary transcriptional effect of FT-6876. We noted 691 genes were differentially expressed (adjusted *p*-value < 0.1); 628 were downregulated and 63 were upregulated. Pathways significantly associated with the 628 repressed genes were *Estrogen Response Early*, *Sox4 Targets Up*, and *MAP Kinase Activity* (adjusted *p* value < 0.1).

Fig. 3 FT-6876 modulates ER and AR target genes in MDA-MB-453 cells. **a** GSEA of RNA-Seq data from MDA-MB-453 cells exposed to 2 μ M FT-6876 for 24 h. **b** ChIP-Seq. Reduction in H3K27Ac and CBP/p300 binding in the promoter region of the ER target gene, AQP3 in MDA-MB-453 cells treated with FT-6876. The area outlined by the dotted green lines indicates the signal induced by R1881 and the impact of FT-6876 on the induced peaks. **c** mRNA expression of AR (SPDEF) and ER (AQP3) target genes was determined by qPCR after exposure to AR agonist R1881 \pm increasing concentrations of FT-6876. AR androgen receptor, ChIP-Seq chromatin immunoprecipitation sequencing, DMSO dimethylsulfoxide, ER estrogen receptor, FDR false discovery rate, GSEA gene set enrichment analysis, NES normalized enrichment scores, qPCR quantitative polymerase chain reaction, RNA-Seq RNA sequencing



In addition to the read-out for transcriptional output at gene bodies, PRO-Seq quantifies transcription genome-wide at coding and noncoding regions alike [32]. Of particular interest is transcription that can be detected at enhancer elements (eRNAs) that harbor high levels of H3K27Ac and occupancy of CBP/p300 assessed using ChIP-Seq [43]. To identify eRNA locations, we used the machine-learning algorithm Transcription Fit (Tfit) to look for sites of bidirectional transcription [44]. As an example, the GATA3 locus harbors a bidirectional transcription start site upstream of its promoter region and itself is significantly repressed by FT-6876 (Fig. 4a). This finding is consistent with the role of the ER in GATA3 expression [45].

Using the Tfit method combined with DeSeq2, we assessed the differential expression status of all bidirectional transcription start sites (Fig. 4b). We noted a significant population of 444 bidirectional transcripts that were significantly downregulated (adjusted p -value $< 10^{-1}$) 1 h following FT-6876 treatment in MDA-MB-453 cells. To search for common transcription factor regulators of these 444 genes, we used the Gene Transcription Regulation Database (GTRD; <https://gtrd.biouml.org/#!>) [46] of curated ChIP-Seq studies combined with the algorithm Giggle [47] to identify significant enrichment of transcription factor binding at these loci. We noted an overwhelmingly significant number of ChIP-Seq studies for the estrogen receptor 1 (ESR1), AR, and CCCTC-binding factor (CTCF) [Fig. 4c]. This complements the previous *Estrogen Response Early* pathway enrichment result computed from the orthogonal differential expression status at gene bodies. Taken together, these PRO-Seq analyses further support the notion that FT-6876 inhibits the transcription of AR and ER target genes.

3.5 FT-6876 Demonstrates a Differential Antiproliferative Effect in AR+ and AR– Breast Cancer Cell Lines

The antiproliferative effect of FT-6876 was evaluated in a time-course study with a washout in a colony formation assay in MDA-MB-453 cells. In this assay, FT-6876 inhibited cell proliferation with an IC_{50} of 100 nM following 10 days of continuous exposure and was approximately 90 times more potent at inhibiting proliferation following 10 days of exposure relative to 3 days and washout, suggesting extended exposure to this class of epigenetic modifiers is necessary to reveal the full extent of the antiproliferative activity (Fig. 5a). We found that 5 days was sufficient to induce the irreversible inhibition of proliferation, although with slightly lower potency than with 10 days of continuous exposure (0.58 μ M and 0.10 μ M, respectively). Enzalutamide, tested side by side with FT-6876, had an IC_{50} of 11.7 μ M following 10 days of continuous exposure and was 45

times less active than FT-6876 at inhibiting proliferation of these AR+ cells (Fig. 5b).

To determine whether sensitivity to FT-6876 is correlated to mRNA expression of AR, the antiproliferative effect of FT-6876 was measured across a panel of 27 breast cancer cell lines with a range of AR expression levels (ESM Table S1). In general, IC_{50} values were low in cell lines with high levels of AR expression, and higher in cell lines with lower levels of AR expression (Fig. 5c).

3.6 FT-6876 Induces Pharmacodynamic and Antitumor Effects in MDA-MB-453 Xenografts In Vivo

The pharmacokinetic profile and pharmacodynamic activity of FT-6876 in vivo were examined in NOD SCID mice bearing MDA-MB-453 xenografts. After a single dose of FT-6876 (10, 30, or 100 mg/kg) was administered, plasma and tumors were collected at different time points over the next 24 h. FT-6876 induced a time- and exposure-dependent reduction in H3K27Ac (Fig. 6a). A single dose of FT-6876 reduced H3K27Ac levels relative to baseline within 2 h, with levels returning to baseline over 24 h (Fig. 6a). Transcription of downstream ER/AR target genes (*XBPI*, *SPDEF*) was also reduced following a single 30 mg/kg dose and tracked with the level of unbound FT-6876 in plasma (Fig. 6b). An immunohistochemical staining analysis in MDA-MB-453 xenografts after 21 days of treatment with FT-6876 showed the modulation of H3K27Ac was maintained for the duration of treatment. The proliferation index (Ki67) was significantly reduced by FT-6876, with mean histoscores of 178 in the vehicle group and 101 in the FT-6876 group (t -statistic = 4.729, two-tailed test; $p < 0.0004$; degrees of freedom = 13) [Fig. 6c]. Pharmacodynamic effects were consistent with the effects on tumor growth in MDA-MB-453 xenografts; long-term treatment with FT-6876 induced tumor stasis in this model (Fig. 6d), whereas body weight remained stable (Fig. 6e).

3.7 FT-6876 Induces Antitumor Effects in Patient-Derived Xenografts

The activity of FT-6876 was evaluated in a panel of PDX models of breast cancer (South Texas Accelerated Research Therapeutics, San Antonio, TX, USA). The panel included 40 tumor models with different AR status across TNBC, HER2, and ER+ subtypes. TGI $> 60\%$ was observed in 20%, 31%, and 38% of ER+, HER2+, and TNBC subtypes, respectively (Figs. 7a, b). When analyzed by AR expression levels (12/39 models were AR+), the proportion of ER+ and TNBC xenografts with high response rates increased to 67% and 50%, respectively, in AR+ models, compared with

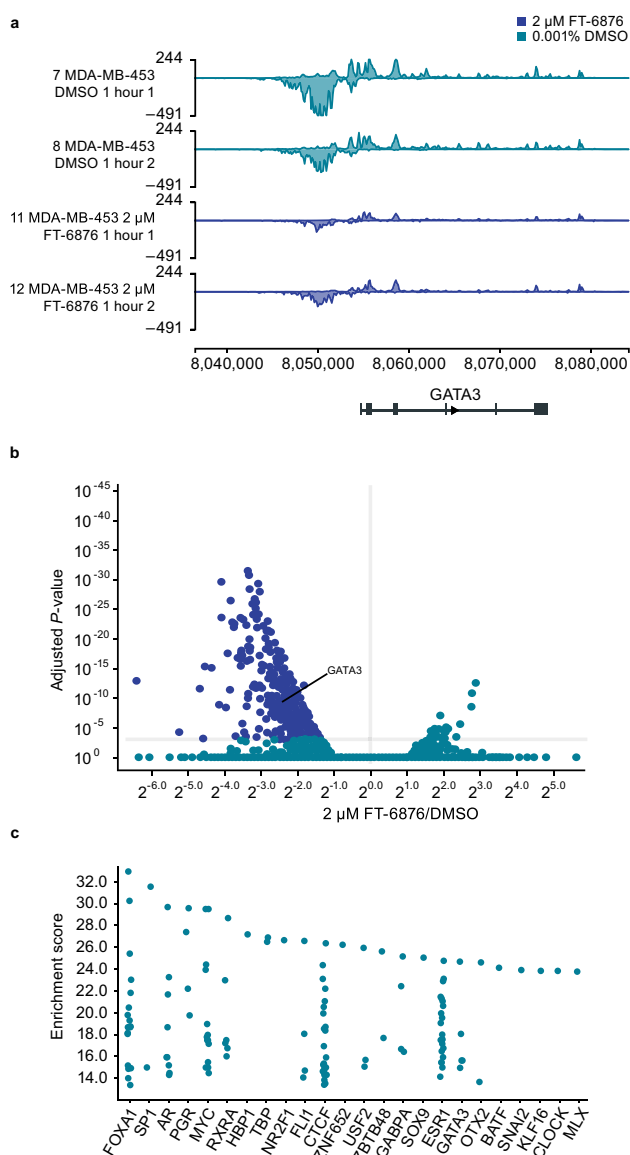


Fig. 4 CBP/p300 inhibition with FT-6876 suggests loss of GATA3 and FOXA1 transcription factor activity. **a** X-axis is the position along the genome (hg38); y-axis is the depth-normalized number of PRO-Seq reads in either DMSO-treated or CBPi-treated MDA-MB-453 cells at the GATA3 locus. **b** Each dot represents a bidirectional transcript; x-axis is log₂-fold change of CBP inhibition over DMSO, and the y-axis refers to significance of that fold-change (adjusted-value). Volcano plot is thresholded at 0.001 to identify differentially expressed transcripts. **c** Bidirectional transcripts arising at both enhancer and promoter regions were mapped across the GTRD database. Each dot represents a ChIP-Seq study, and the y-axis refers to the enrichment score representing the overlap between the bidirectional transcripts from PRO-Seq and the ChIP-Seq peaks. Significance is calculated using the Giggle Algorithm. *ChIP-Seq* chromatin immunoprecipitation sequencing, *DMSO* dimethylsulfoxide, *GTRD* Gene Transcription Regulation Database

0% and 41% in AR low models. Results of the study using patient-derived tumor models further support our hypothesis that AR+ breast cancer cells are more sensitive to CBP/p300 inhibition.

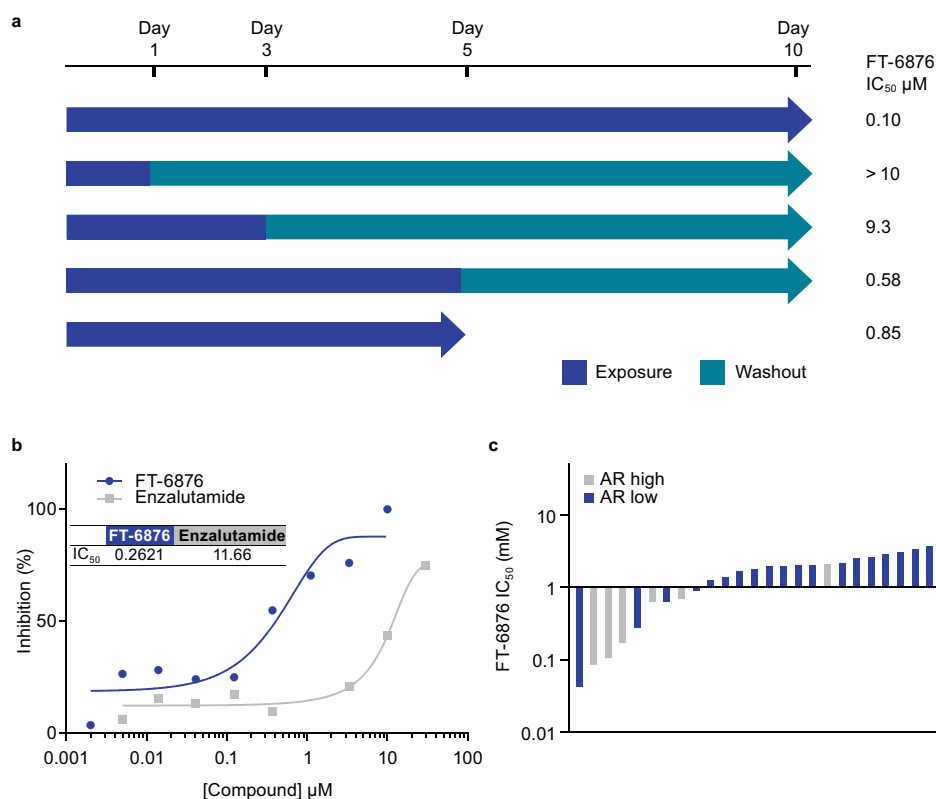
4 Discussion

Breast cancer is the most common type of cancer in women, with rates surpassing lung cancer [48]. The International Agency for Research on Cancer estimates there were 2.3 million cases of breast cancer and more than 680,000 deaths globally in 2020 [48]. The most aggressive subtype of breast cancer, TNBC, has limited treatment options; these tumors are refractory to hormone therapy due to the lack of ER and PR expression, as well as a lack of HER2 amplification [5]. The recent approval of PARP inhibitors and immune checkpoint modulators for the treatment of TNBC increases treatment options for these patients, although additional targeted therapies are needed [49]. Traditionally, drugs targeting transcription factors and their co-activators have been challenging to develop, although advances over the last several years in the design and development of small-molecule inhibitors of BRDs, initially targeting the BET family, have stimulated efforts toward finding inhibitors of additional BRDs [50, 51].

In this study, we present FT-6876, a novel, potent, and selective small-molecule inhibitor of the BRDs of CBP/p300. These highly related multidomain proteins catalyze the acetylation of histone and nonhistone proteins. The AR is an example of a nonhistone substrate of acetylation, which stabilizes the protein and increases AR signaling [14, 16, 52]. Indeed, mutations at specific lysine residues on AR that mimic acetylation have been shown to increase both the expression of specific AR genes involved in the cell cycle (i.e., genes encoding cyclin D1 and cyclin E) and prostate cancer cell proliferation [23]. Our results demonstrated FT-6876 rapidly and reversibly reduced H3K27Ac in AR+ cells, thereby reflecting the dynamic state of histone modification in cells. High-content analysis confirmed the reduction in H3K27Ac occurred uniformly across the population of cells. This confirmed the proposed activity and is consistent with findings for CBP30, another CBP/p300 inhibitor, that decreased the level of H3K27Ac at AR-binding sites in MDA-MB-453 cells [53].

Results from ChIP-Seq, RNA-Seq, and PRO-Seq studies reported in this current study support the proposed mechanism of action, whereby FT-6876 displaces CBP/p300 from chromatin, thus reducing H3K27Ac and target

Fig. 5 Antiproliferative effect of FT-6876. **a** Time-dependent growth inhibition in a colony formation assay in MDA-MB-453 cells. **b** Inhibition of MDA-MB-453 cellular growth after 10 days of continuous exposure to FT-6876 or enzalutamide. **c** Effect of FT-6876 in a panel of 27 breast cancer cell lines with a range of AR expression levels (ESM Table S1). AR androgen receptor, IC_{50} half maximal inhibitory concentration



gene expression. Reduction of H3K27Ac at the regulatory region of the ER target gene *AQP3* was associated with the concomitant decrease in CBP and p300 occupancy at this site and a reduction in the mRNA level of this gene. GSEA revealed impacts of the compound on Myc, cell cycle (E2F), ER, and AR pathways in line with the inhibition of proliferation in cell lines in vitro and tumor growth in PDX models in vivo. We observed a preferential effect of sensitivity to FT-6876 on AR+ cell lines in vitro and patient-derived models in vivo. The dose-dependent modulation of proximal and distal pharmacodynamic biomarkers, H3K27Ac and ER/AR genes translated into a dose-dependent TGI.

This study has several limitations. The current manuscript provides significant evidence of the displacement of CBP and p300 from chromatin with FT-6876. Other reports in the literature have already shown significant evidence of the structure of CBP and p300 and the interaction between the bromodomain and the histone acetyl transferase domain [21, 54]; therefore, it has not been included in our report. FT-6876 would be a suitable candidate for further characterization of the structural rearrangement induced by binding of the compound. A further limitation of this work is that the studies on the cellular mechanism of action of FT-6876 rely on immortalized human cancer cell lines, which may not fully recapitulate the activity of the compound in human disease. This limitation has been somewhat mitigated by the demonstration of anti-tumor activity of FT-6876 in a panel

of human PDX models in vivo. In addition, although the PDX screen indicates an enrichment of responsive models in AR+ PDX models, future studies would need to address patient selection options for the clinical study. Determination of AR status in breast cancer using immunohistochemistry has been the subject of several publications [55, 56] and should be further characterized for FT-6876. Finally, a potential option for patient selection is to build on the results from the PDX screen and develop a gene signature to be used in clinical studies.

5 Conclusion

We have discovered FT-6876, a novel inhibitor of the bromodomain of CBP/p300. Our results confirm the proposed mechanism of action of FT-6876. Disruption of AR signaling via the inhibition of CBP/p300 BRD provides an alternative mechanism for the modulation of AR- and ER-dependent transcription to complement direct antagonism of the receptor–ligand interaction. Taken together, our results support the use of FT-6876 to study the biology of CBP/p300 in the context of nuclear hormone receptor regulation. Clinical trials to test this hypothesis are ongoing with the investigational CBP/p300 inhibitors FT-7051 (NCT04575766) and CCS-1477 (NCT03568656).

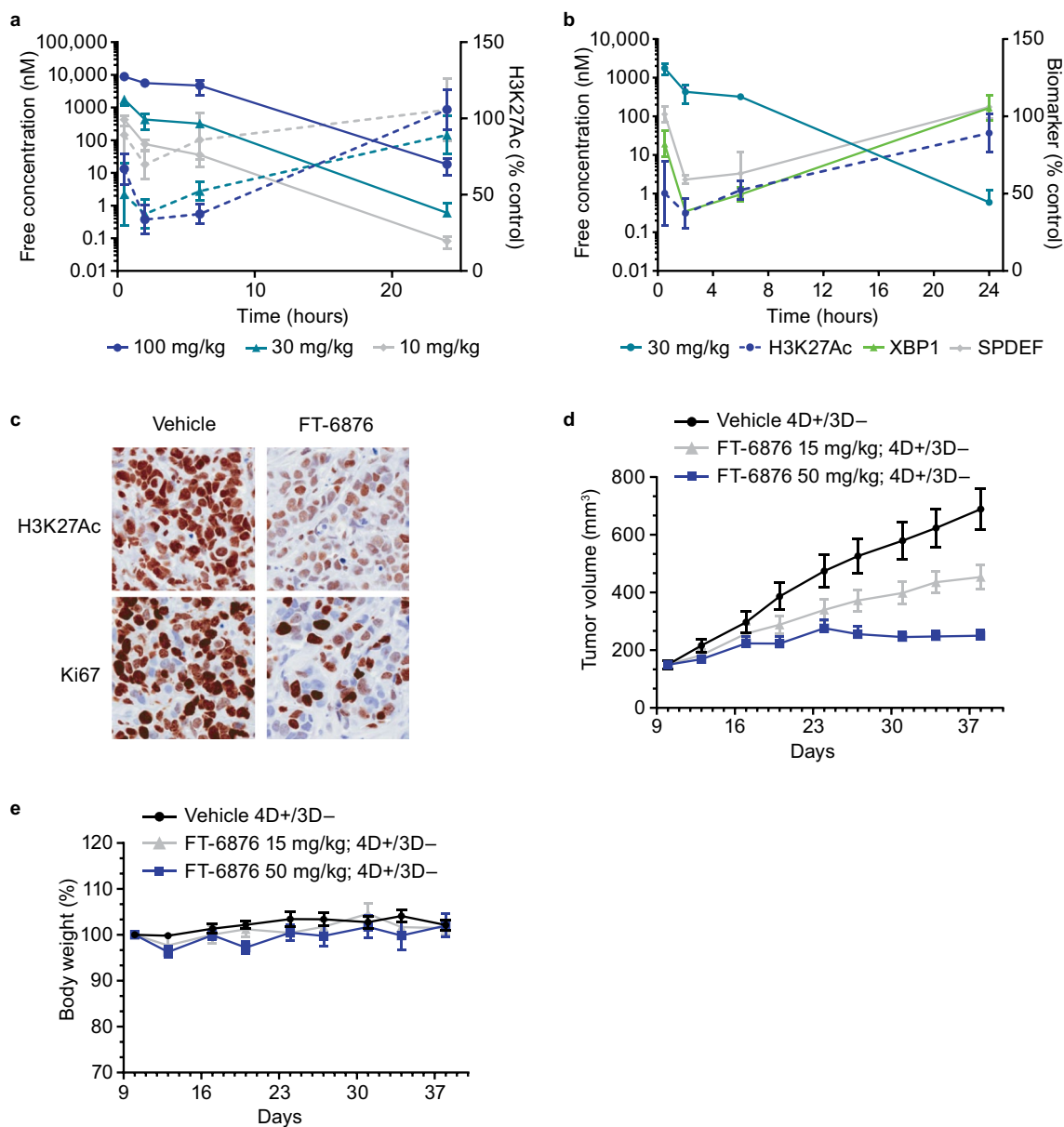
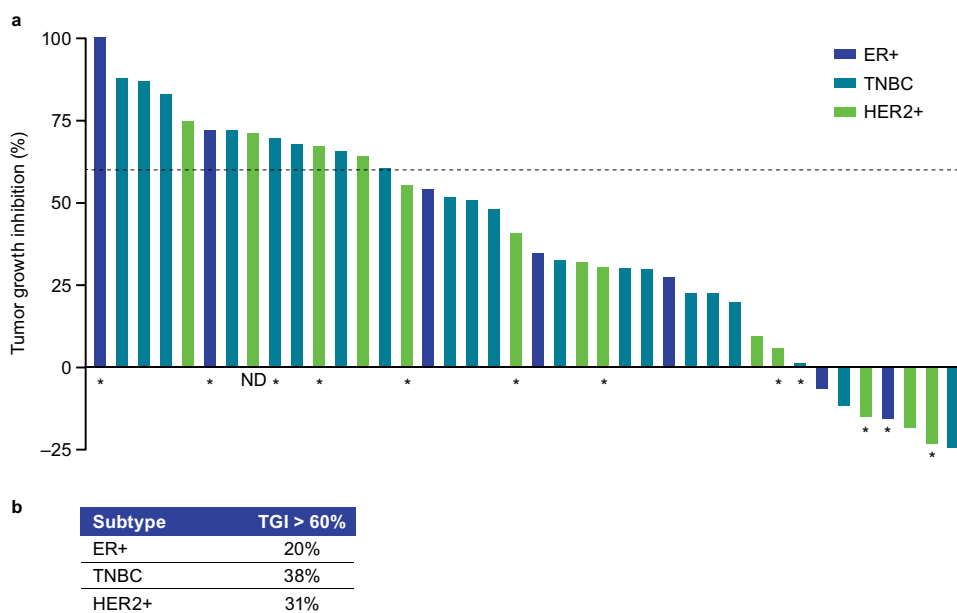


Fig. 6 FT-6876 induces pharmacodynamic and antitumor effects in MDA-MB-453 xenografts. **a** The plasma concentration of FT-6876 and H3K27Ac was measured in NOD SCID mice bearing MDA-MB-453 xenografts after a range of FT-6876 doses. Solid lines show free plasma concentration of FT-6876, and dotted lines show H3K27Ac tumor levels expressed as percentage control. **b** After a single FT-6876 30 mg/kg dose, free plasma concentration of FT-6876

and H3K27Ac, as well as transcription of downstream ER/AR target genes (*XBP1*, *SPDEF*), were measured in tumors. **c** Representative images of tumor areas stained for Ki67 and H3K27Ac. **d**, **e** Tumor volumes and mouse body weight, respectively, measured over time in the different cohorts of animals. *AR* androgen receptor, *ER* estrogen receptor, *NOD* nonobese diabetic, *SCID* severe combined immunodeficiency

Fig. 7 High response rate in patient-derived xenografts with AR+ TNBC and ER+ tumors. In vivo efficacy screen in a panel of START Patient-Derived Xenograft (START-PDX) models representing human breast cancer, in immune-deficient mice. **a** The bars represent the TGI for each model tested. A threshold of 60% TGI was used to discriminate responsive from nonresponsive models. Asterisks represent AR+ expression. **b** Response rates per breast cancer subtypes. AR androgen receptor, ER estrogen receptor, HER2+ human epidermal growth factor receptor 2-positive, ND not determined, TGI tumor growth inhibition, TNBC triple-negative breast cancer



Supplementary Information The online version contains supplementary material available at <https://doi.org/10.1007/s11523-023-00949-7>.

Acknowledgments Medical writing assistance was provided by Geraldine Thompson and Sue Reinwald, of Engage Scientific Solutions, Horsham, UK, and Connecticut, USA, respectively, which was funded by Forma Therapeutics, Inc., Watertown, MA, USA.

Declarations

Funding This study was funded by Forma Therapeutics, Inc., Watertown, MA, USA.

Author contributions Conceptualization: AC, AT, EW, GLW, JC, KWW, MC, PL, QX, SMG, SS, and TH. Data curation: BG, JA, LY, MC, and SMG. Formal analysis: BG, EW, JA, JC, LB, MC, and SMG. Investigation: AC, AT, BG, EP, EW, JB, JC, LB, LY, MC, ML, PL, SMG, and SS. Methodology: GLW, JA, JC, MC, QX, SMG, SS, and TH. Project administration: MC, SMG, PL, GLW, KWW, QX, LY, and SS. Resources: GLW, JC, LB, and LY. Software: JA. Validation: AC, EW, JC, LB, LY, SMG, and SS. Visualization: MC specifically developed the figures. TH generated de novo design visualization and authored the section describing the inception and design of FT-6876, which outlines the chemistry of intermediates and proof-of-concept molecules. JC and SMG also contributed to data visualization. Supervision: EW, GLW, LY, MC, and SMG. Writing – review and editing: All authors reviewed and approved the manuscript.

Conflicts of interest Kenneth W. Wood and Sylvia M. Guichard declare they are employees of and hold stock in Forma Therapeutics, Inc. Maureen Caligiuri is an employee of Forma Therapeutics, Inc., and declares the provision of writing assistance, medicines, or administrative support and affirms patents (WO 2020/190792, Compositions and methods for treating AR+ forms of cancer; US 2022/0088005A, Bromodomain inhibitors for AR-driven cancers). Grace L. Williams declares having owned stock in Forma Therapeutics, Inc. within the last 36 months. Ping Li declares past employment with Forma Therapeutics, Inc. (until February 2019). Jennifer Castro was an employee

of Forma Therapeutics, Inc. at the time of the study. Angela Toms declares patents as well as stock ownership generated via the normal course of employment with Forma Therapeutics, Inc. Eneida Pardo, Joel Basken, Linda Battalagine, Erik Wilker, Lili Yao, Shawn Schiller, Agustin Chicas, Maria Lai, and Bradford Graves declare no conflicts of interest within the past 36 months. Joey Azofeifa is an employee and founder of Arpeggio Bio, which was contracted by Forma Therapeutics, Inc. to undertake the PRO-Seq experiments described in this paper. Torsten Herbertz declares previous (until February 2019) employment with Forma Therapeutics Inc., stock ownership based on the conversion of incentive equity grants after an initial public offering in 2020, and patents as the inventor of FT-6876 and the related molecule FT-7051 (WO2019055877A1, WO2019055869A1, WO2020006483A1, US11,292,791, WO2020190791, US20200002332). Qunli Xu declares having owned stock in Forma Therapeutics, Inc., and a patent application assigned to Forma Therapeutics, Inc.

Ethics Approval All the procedures related to animal care were performed according to guidelines approved by the Institutional Animal Care and Use Committee of Pharmaron following the guidance of the Association for Assessment and Accreditation of Laboratory Animal Care.

Consent to participate and publish Not applicable due to the study being preclinical in nature.

Data and materials availability All data associated with this study are presented in the main text or the electronic supplementary material.

Code availability Not applicable.

Open Access This article is licensed under a Creative Commons Attribution-NonCommercial 4.0 International License, which permits any non-commercial use, sharing, adaptation, distribution and reproduction in any medium or format, as long as you give appropriate credit to the original author(s) and the source, provide a link to the Creative Commons licence, and indicate if changes were made. The images or other third party material in this article are included in the article's Creative Commons licence, unless indicated otherwise in a credit line to the material. If material is not included in the article's Creative Commons

licence and your intended use is not permitted by statutory regulation or exceeds the permitted use, you will need to obtain permission directly from the copyright holder. To view a copy of this licence, visit <http://creativecommons.org/licenses/by-nc/4.0/>.

References

- Morris GJ, Naidu S, Topham AK, Guiles F, Xu Y, McCue P, et al. Differences in breast carcinoma characteristics in newly diagnosed African-American and Caucasian patients: a single-institution compilation compared with the National Cancer Institute's Surveillance, Epidemiology, and End Results database. *Cancer*. 2007;110:876–84.
- Lehmann BD, Bauer JA, Chen X, Sanders ME, Chakravarthy AB, Shyr Y, et al. Identification of human triple-negative breast cancer subtypes and preclinical models for selection of targeted therapies. *J Clin Invest*. 2011;121:2750–67.
- Robinson JL, Macarthur S, Ross-Innes CS, Tilley WD, Neal DE, Mills IG, et al. Androgen receptor driven transcription in molecular apocrine breast cancer is mediated by FoxA1. *EMBO J*. 2011;30:3019–27.
- Lehmann BD, Jovanovic B, Chen X, Estrada MV, Johnson KN, Shyr Y, et al. Refinement of triple-negative breast cancer molecular subtypes: implications for neoadjuvant chemotherapy selection. *PLoS ONE*. 2016;11: e0157368.
- Mina A, Yoder R, Sharma P. Targeting the androgen receptor in triple-negative breast cancer: current perspectives. *Onco Targets Ther*. 2017;10:4675–85.
- Dieci MV, Tsvetkova V, Griguolo G, Miglietta F, Mantiero M, Tasca G, et al. Androgen receptor expression and association with distant disease-free survival in triple negative breast cancer: analysis of 263 patients treated with standard therapy for stage I-III disease. *Front Oncol*. 2019;9:452.
- Traina TA, Miller K, Yardley DA, Eakle J, Schwartzberg LS, O'Shaughnessy J, et al. Enzalutamide for the treatment of androgen receptor-expressing triple-negative breast cancer. *J Clin Oncol*. 2018;36:884–90.
- Carroll JS. Mechanisms of oestrogen receptor (ER) gene regulation in breast cancer. *Eur J Endocrinol*. 2016;175:R41–9.
- Peyraud F, Italiano A. Combined PARP inhibition and immune checkpoint therapy in solid tumors. *Cancers (Basel)*. 2020;12:1502.
- Amos KD, Adamo B, Anders CK. Triple-negative breast cancer: an update on neoadjuvant clinical trials. *Int J Breast Cancer*. 2012;2012: 385978.
- Barton VN, D'Amato NC, Gordon MA, Christenson JL, Elias A, Richer JK. Androgen receptor biology in triple negative breast cancer: a case for classification as AR+ or quadruple negative disease. *Horm Cancer*. 2015;6:206–13.
- Sharp PP, Garnier J-M, Huang DCS, Burns CJ. Evaluation of functional groups as acetyl-lysine mimetics for BET bromodomain inhibition. *MedChemComm*. 2014;5:1834–42.
- Abramovitch R, Tavor E, Jacob-Hirsch J, Zeira E, Amarglio N, Pappo O, et al. A pivotal role of cyclic AMP-responsive element binding protein in tumor progression. *Cancer Res*. 2004;64:1338–46.
- Fu M, Wang C, Reutens AT, Wang J, Angeletti RH, Siconolfi-Baez L, et al. p300 and p300/cAMP-response element-binding protein-associated factor acetylate the androgen receptor at sites governing hormone-dependent transactivation. *J Biol Chem*. 2000;275:20853–60.
- Shankar DB, Cheng JC, Kinjo K, Federman N, Moore TB, Gill A, et al. The role of CREB as a proto-oncogene in hematopoiesis and in acute myeloid leukemia. *Cancer Cell*. 2005;7:351–62.
- Waddell AR, Huang H, Liao D. CBP/p300: critical co-activators for nuclear steroid hormone receptors and emerging therapeutic targets in prostate and breast cancers. *Cancers (Basel)*. 2021;13:2872.
- Mantelingu K, Reddy BA, Swaminathan V, Kishore AH, Sid-dappa NB, Kumar GV, et al. Specific inhibition of p300-HAT alters global gene expression and represses HIV replication. *Chem Biol*. 2007;14:645–57.
- Zucconi BE, Makofske JL, Meyers DJ, Hwang Y, Wu M, Kuroda MI, et al. Combination targeting of the bromodomain and acetyltransferase active site of p300/CBP. *Biochemistry*. 2019;58:2133–43.
- Zaware N, Zhou MM. Bromodomain biology and drug discovery. *Nat Struct Mol Biol*. 2019;26:870–9.
- Jin L, Garcia J, Chan E, de la Cruz C, Segal E, Merchant M, et al. Therapeutic targeting of the CBP/p300 bromodomain blocks the growth of castration-resistant prostate cancer. *Cancer Res*. 2017;77:5564–75.
- Park S, Stanfield RL, Martinez-Yamout MA, Dyson HJ, Wilson IA, Wright PE. Role of the CBP catalytic core in intramolecular SUMOylation and control of histone H3 acetylation. *Proc Natl Acad Sci USA*. 2017;114:E5335–42.
- Fronsdal K, Engedal N, Slagsvold T, Saatcioglu F. CREB binding protein is a coactivator for the androgen receptor and mediates cross-talk with AP-1. *J Biol Chem*. 1998;273:31853–9.
- Fu M, Rao M, Wang C, Sakamaki T, Wang J, Di Vizio D, et al. Acetylation of androgen receptor enhances coactivator binding and promotes prostate cancer cell growth. *Mol Cell Biol*. 2003;23:8563–75.
- McLure KG, Gesner EM, Tsujikawa L, Kharenko OA, Attwell S, Campeau E, et al. RVX-208, an inducer of ApoA-I in humans, is a BET bromodomain antagonist. *PLoS ONE*. 2013;8: e83190.
- Zhong J, Ding L, Bohrer LR, Pan Y, Liu P, Zhang J, et al. p300 acetyltransferase regulates androgen receptor degradation and PTEN-deficient prostate tumorigenesis. *Cancer Res*. 2014;74:1870–80.
- Wen S, Niu Y, Huang H. Posttranslational regulation of androgen dependent and independent androgen receptor activities in prostate cancer. *Asian J Urol*. 2020;7:203–18.
- Kanayama M, Lu C, Luo J, Antonarakis ES. AR splicing variants and resistance to AR targeting agents. *Cancers (Basel)*. 2021;13:2563.
- Welti J, Sharp A, Brooks N, Yuan W, McNair C, Chand SN, et al. Targeting the p300/CBP axis in lethal prostate cancer. *Cancer Discov*. 2021;11:1118–37.
- Lasko LM, Jakob CG, Edalji RP, Qiu W, Montgomery D, Digiammarino EL, et al. Discovery of a selective catalytic p300/CBP inhibitor that targets lineage-specific tumours. *Nature*. 2017;550:128–32.
- Romero FA, Murray J, Lai KW, Tsui V, Albrecht BK, An L, et al. GNE-781, A highly advanced potent and selective bromodomain inhibitor of cyclic adenosine monophosphate response element binding protein, binding protein (CBP). *J Med Chem*. 2017;60:9162–83.
- Yang Y, Zhang R, Li Z, Mei L, Wan S, Ding H, et al. Discovery of highly potent, selective, and orally efficacious p300/CBP histone acetyltransferases inhibitors. *J Med Chem*. 2020;63:1337–60.
- Mahat DB, Kwak H, Booth GT, Jonkers IH, Danko CG, Patel RK, et al. Base-pair-resolution genome-wide mapping of active RNA polymerases using precision nuclear run-on (PRO-seq). *Nat Protoc*. 2016;11:1455–76.

33. Denny RA, Flick AC, Coe J, Langille J, Basak A, Liu S, et al. Structure-based design of highly selective inhibitors of the CREB binding protein bromodomain. *J Med Chem*. 2017;60:5349–63.
34. Hammitzsch A, Tallant C, Fedorov O, O'Mahony A, Brennan PE, Hay DA, et al. CBP30, a selective CBP/p300 bromodomain inhibitor, suppresses human Th17 responses. *Proc Natl Acad Sci U S A*. 2015;112:10768–73.
35. Hay DA, Fedorov O, Martin S, Singleton DC, Tallant C, Wells C, et al. Discovery and optimization of small-molecule ligands for the CBP/p300 bromodomains. *J Am Chem Soc*. 2014;136:9308–19.
36. Filippakopoulos P, Picaud S, Mangos M, Keates T, Lambert JP, Barsyte-Lovejoy D, et al. Histone recognition and large-scale structural analysis of the human bromodomain family. *Cell*. 2012;149:214–31.
37. Lolli G, Battistutta R. Different orientations of low-molecular-weight fragments in the binding pocket of a BRD4 bromodomain. *Acta Crystallogr D Biol Crystallogr*. 2013;69:2161–4.
38. Picaud S, Wells C, Felletar I, Brotherton D, Martin S, Savitsky P, et al. RVX-208, an inhibitor of BET transcriptional regulators with selectivity for the second bromodomain. *Proc Natl Acad Sci USA*. 2013;110:19754–9.
39. Bamborough P, Diallo H, Goodacre JD, Gordon L, Lewis A, Seal JT, et al. Fragment-based discovery of bromodomain inhibitors part 2: optimization of phenylisoxazole sulfonamides. *J Med Chem*. 2012;55:587–96.
40. Chung CW, Dean AW, Woolven JM, Bamborough P. Fragment-based discovery of bromodomain inhibitors part 1: inhibitor binding modes and implications for lead discovery. *J Med Chem*. 2012;55:576–86.
41. Fish PV, Filippakopoulos P, Bish G, Brennan PE, Bunnage ME, Cook AS, et al. Identification of a chemical probe for bromo and extra C-terminal bromodomain inhibition through optimization of a fragment-derived hit. *J Med Chem*. 2012;55:9831–7.
42. von Mikecz A, Zhang S, Montminy M, Tan EM, Hemmerich P. CREB-binding protein (CBP)/p300 and RNA polymerase II colocalize in transcriptionally active domains in the nucleus. *J Cell Biol*. 2000;150:265–73.
43. Fox S, Myers JA, Davidson C, Getman M, Kingsley PD, Frankiewicz N, et al. Hyperacetylated chromatin domains mark cell type-specific genes and suggest distinct modes of enhancer function. *Nat Commun*. 2020;11:4544.
44. Azofeifa JG, Dowell RD. A generative model for the behavior of RNA polymerase. *Bioinformatics*. 2017;33:227–34.
45. Eeckhoutte J, Keeton EK, Lupien M, Krum SA, Carroll JS, Brown M. Positive cross-regulatory loop ties GATA-3 to estrogen receptor alpha expression in breast cancer. *Cancer Res*. 2007;67:6477–83.
46. Yevshin I, Sharipov R, Kolmykov S, Kondrakhin Y, Kolpakov F. GTRD: a database on gene transcription regulation-2019 update. *Nucleic Acids Res*. 2019;47:D100–5.
47. Layer RM, Pedersen BS, DiSera T, Marth GT, Gertz J, Quinlan AR. GIGGLE: a search engine for large-scale integrated genome analysis. *Nat Methods*. 2018;15:123–6.
48. Sung H, Ferlay J, Siegel RL, Laversanne M, Soerjomataram I, Jemal A, et al. Global cancer statistics 2020: GLOBOCAN estimates of incidence and mortality worldwide for 36 cancers in 185 countries. *CA Cancer J Clin*. 2021;71:209–49.
49. Shen M, Pan H, Chen Y, Xu YH, Yang W, Wu Z. A review of current progress in triple-negative breast cancer therapy. *Open Med (Wars)*. 2020;15:1143–9.
50. Cochran AG, Conery AR, Sims RJ 3rd. Bromodomains: a new target class for drug development. *Nat Rev Drug Discov*. 2019;18:609–28.
51. Doroshow DB, Eder JP, LoRusso PM. BET inhibitors: a novel epigenetic approach. *Ann Oncol*. 2017;28:1776–87.
52. Faus H, Haendler B. Androgen receptor acetylation sites differentially regulate gene control. *J Cell Biochem*. 2008;104:511–24.
53. Garcia-Carpizo V, Ruiz-Llorente S, Sarmentero J, Gonzalez-Corpas A, Barrero MJ. CREBBP/EP300 bromodomain inhibition affects the proliferation of AR-positive breast cancer cell lines. *Mol Cancer Res*. 2019;17:720–30.
54. Delvecchio M, Gaucher J, Aguilar-Gurrieri C, Ortega E, Panne D. Structure of the p300 catalytic core and implications for chromatin targeting and HAT regulation. *Nat Struct Mol Biol*. 2013;20:1040–6.
55. Kumar V, Yu J, Phan V, Tudor IC, Peterson A, Uppal H. Androgen receptor immunohistochemistry as a companion diagnostic approach to predict clinical response to enzalutamide in triple-negative breast cancer. *JCO Precis Oncol*. 2017;1:1–19.
56. Liu YX, Zhang KJ, Tang LL. Clinical significance of androgen receptor expression in triple negative breast cancer—an immunohistochemistry study. *Oncol Lett*. 2018;15:10008–16.